Marine Micropaleontology 186 (2024) 102308

Contents lists available at ScienceDirect

Marine Micropaleontology

journal homepage: www.elsevier.com/locate/marmicro

The origin and significance of euhedral apatite crystals on conodonts

Daniele Malferrari [a], Annalisa Ferretti [a,*], Luca Medici [b]

[a] Department of Chemical and Geological Sciences, University of Modena and Reggio Emilia, Via Campi 103, 41125 Modena, Italy
[b] National Research Council of Italy, Institute of Methodologies for Environmental Analysis, C. da S. Loja-Zona Industriale, 85050 Tito Scalo, Potenza, Italy

ARTICLE INFO

Keywords:
Biomineralization
Bioapatite
Conodonts
Euhedral apatite
Diagenesis
HFSE
REE
Ordovician

ABSTRACT

Crystal overgrowth on fossil remains is well-documented in the literature. Attention has specifically focused on bioapatite (*i.e.*, an apatite of biochemical origin regardless of post-mortem changes) configurations, in order to decipher any possible relation to fossilization/diagenesis. This study investigates the Rare Earth Element (REE) and other High-Field-Strength Element (HFSE) composition of euhedral crystals formed on the surface of conodont elements compared with that of crystal-free surfaces. Euhedral crystals are by definition crystals characterized by sharp faces, developing solids that, for apatite, assume the form of hexagonal prisms, reflecting its crystal symmetry. Late Ordovician (*Amorphognathus ordovicicus* Zone) conodonts from two localities in Sardinia and the Carnic Alps (Italy) are herein investigated. Conodont elements reveal the occurrence of smooth surfaces and surfaces partially covered with euhedral crystals. Since euhedral crystals did not reasonably grow during the organism's lifetime, the REE and HFSE analysis can provide important insights into the crystal growth process. The experimental results indicated a substantial contribution of diagenetic imprinting for all the analyzed material, although more evident on euhedral crystals that are significantly enriched in middle and, subordinately, in heavy REE with respect to smooth surfaces. The positive correlations between La + Th *vs* log[ΣREE] and Ce + Th *vs* log[ΣREE] could support the hypothesis that the neoformed euhedral crystals grew also by depleting the pristine bioapatite of the conodont elements. Nevertheless, the occurrence of two types of apatite cannot be ruled out: euhedral crystals as neoformed products of diagenetic processes and smooth surfaces as remains of the pristine conodont bioapatite after diagenesis.

1. Introduction

Conodont elements represent valuable archives of sea/pore water chemistry; yet they often show evidence of diagenetic mineral overgrowth which may be biasing measurements. Elements are composed of calcium phosphate with a fluorine-hydroxyapatite [$Ca_5(PO_4,CO_3)_3(F,OH)$] like structure; because of its strictly biochemical origin, it is usually referred to as bioapatite, regardless of the *post-mortem* changes (Keenan et al., 2015; Skinner, 2005). Distinctive features of bioapatite include the possible chemical, iso- and hetero-valent substitutions that can occur at the anionic and cationic sites both throughout the lifetime of the organism and during burial and *post mortem* diagenesis (Zapanta LeGeros, 1981). For example, the phosphate anion can be replaced by carbonate, as can hydroxyl by fluorine or chlorine (the latter rarer in a sedimentary environment); calcium, in turn, can be replaced by sodium and potassium (Brigatti et al., 2004; Ferretti et al., 2021; Keenan and Engel, 2017), but also by Rare Earth Elements (REE) and other High-Field-Strength Elements (HFSE) (Ferretti et al., 2023a; Grandjean-Lécuyer et al., 1993; Li et al., 2017; Reynard et al., 1999; Trotter et al., 2007; Trotter and Eggins, 2006; Trueman and Tuross, 2002; Zhao et al., 2013). Although not without controversial views, the contents of REE and HFSE have been widely used for paleoenvironmental reconstructions and, most importantly, to detect any diagenetic footprint (Armstrong et al., 2001; Chen et al., 2015; Herwartz et al., 2013; Holser, 1997; Kocsis et al., 2010; Liao et al., 2019; Medici et al., 2021; Picard et al., 2002; Reynard et al., 1999; Toyoda and Tokonami, 1990; Trotter et al., 2016; Trotter and Eggins, 2006; Zhang et al., 2016; Zhao et al., 2013; Žigaitė et al., 2020). In fact, in view of the short lifespan of an organism compared to geological times, it is during diagenesis that bioapatite is most chemically modified (Chen et al., 2015; Kim et al., 2012; Lécuyer et al., 2004; Trotter et al., 2016; Zhang et al., 2016) and a frank estimation of REE sources can be based, for example, on the analysis of specific relationships between the sum of all REE (ΣREE), light REE (LREE), middle REE (MREE), heavy REE (HREE) and the content of Y and Ho (Chen et al., 2015; Grandjean-Lécuyer et al., 1993; Lécuyer et al., 2004; Li et al., 2017; Nothdurft et al., 2004; Nozaki et al.,

* Corresponding author.
E-mail address: ferretti@unimore.it (A. Ferretti).

https://doi.org/10.1016/j.marmicro.2023.102308
Received 23 August 2023; Received in revised form 4 November 2023; Accepted 9 November 2023
Available online 11 November 2023

1997; Pattan et al., 2005; Peppe and Reiners, 2007; Shen et al., 2012; Webb et al., 2009; Webb and Kamber, 2000; Wright et al., 1987; Wright and Colling, 1995; Zhang et al., 1994, 2016; Zhang and Nozaki, 1996). Some studies have considered the influence on fossil chemical compositions of the depositional environment with respect to diet or physiology of vertebrates, underlying that they are variously affected by the stages of diagenesis. For example, Lécuyer et al. (2003) studied phosphatic remains from faunal associations of the Upper Cretaceous continental and marine sediments of northern Spain, proposing that the geochemistry of these vertebrate remains reflects the geochemistry of the depositional environment. Likewise, REE patterns of different fossil remains highlighted the role of early diagenesis in defining the chemistry of the phosphatic remains (Fadel et al., 2015; Lécuyer et al., 2003; Žigaitė et al., 2015). Similarly, fossil vertebrate microremains from the Lower Devonian of Svalbard (Žigaitė et al., 2016) and from the lower Silurian of Estonia (Fadel et al., 2015) evidenced the importance of *in situ* measurements, showing different REE concentrations in various dental tissues. Conversely, minor differences in REE content among various conodont morphotypes (Medici et al., 2021) and/or histologies (Fadel et al., 2015; Žigaitė et al., 2015, 2016) suggest looking for variations among the possible types of apatite occurring on the fossil surfaces.

Therefore, this research focuses on a peculiarity that is not very common, but not so rare either, which is the occurrence of neoformed euhedral (or subhedral) apatite crystals on the surface of conodont elements. Euhedral crystals, also known as idiomorphic (subidiomorphic) crystals, are crystals that, regardless of size, exhibit sharp and easily recognizable faces, forming solids that sometimes mirror the internal symmetry of the lattice (*i.e.*, the symmetric distribution of the atoms that characterize crystals) of the mineral they represent (for example, in the case of apatite, euhedral crystals show a hexagonal prismatic habit). When only a portion of the solid is formed, then we speak of subhedral crystals (*e.g.*, a portion of a hexagonal prism for apatite). Two necessary (but not sufficient) conditions for the development of euhedral crystals are the availability of space and the disposability of chemical elements for crystal growth. The latter may provide insight into the origin of the chemical elements of the crystals, especially trace elements.

Conodont elements from two classical Late Ordovician localities, Cannamenda (southwestern Sardinia, Italy) and Monte Zermula (Carnic Alps, northeastern Italy), were considered (Fig. 1). The two areas have been under study for many years by members of our research group, have a precise biostratigraphic assignment and provided a rich and well-diversified conodont collection including either global or endemic taxa.

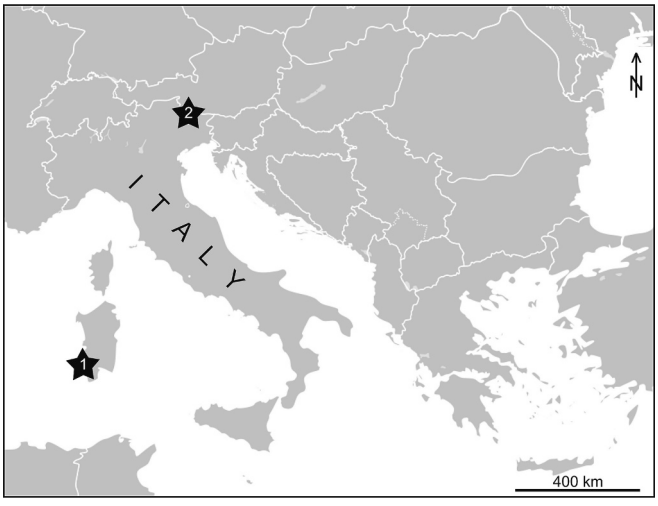

Fig. 1. Location of the two spots investigated in this study. 1: Cannamenda, SW Sardinia, Italy (coordinates 39°14′07.1" N 8°29′18.0" E); 2: Monte Zermula, Carnic Alps, NE Italy (coordinates 46°33′41.29" N 13°09′05.98" E).

Specimens recovered from both localities show element surfaces partially or totally covered with euhedral crystals sometimes replacing cusps and/or process denticles, or surfaces completely smooth. The specimens were first characterized under scanning electron microscopy (SEM) in order to identify "smooth" and "euhedral crystal" areas, that were later analyzed for REE and other HFSE composition through laser ablation inductively coupled mass spectrometry (LA-ICPMS). For the purpose of this research, subhedral crystals can be considered as euhedral crystals whose growth was interrupted, and in the following we will not distinguish them further and refer to euhedral crystals only. Regarding smooth surfaces, measurements were performed on the outermost part of the element wall.

It is rationale to suppose that euhedral crystals did not form during the life of the organism but have rather grown during diagenesis. Since no dependence on paleogeographic provenance, CAI, or taxonomy exists (Ferretti et al., 2017), the analysis of trace elements may provide important indications on *mode* and *tempo* of apatite crystal growth. More specifically, by comparing the differences in REE concentration (*i.e.*, specific correlations between them) in euhedral crystals and in smooth surfaces, it might be possible to discriminate the diagenetic imprint on the original tissues (bioapatite) compared to the pure outcome of diagenesis (euhedral apatite crystals).

2. Geological setting

Ordovician sedimentary and volcanic successions are extensively exposed in Italy in Sardinia and, to a lesser extent, in the Carnic Alps. We will briefly illustrate main geological features of the two investigated areas, but we refer respectively to Loi et al. (2023) and Ferretti et al. (2023a) for a more detailed report on the two geographic sectors.

2.1. Cannamenda, SW Sardinia

The Ordovician successions are exposed in Sardinia (locality 1 in Fig. 1) in several parts of the island, but with remarkable differences between SW Sardinia (External Zone), considered to be a para-autochthonous section, and the rest of Sardinia (Nappe Zone and Inner Zone). In the Sulcis-Iglesiente Unit, to which our deposits belong, an intra-Ordovician unconformity (Sardic Unconformity; Teichmüller, 1931) separates the lower Cambrian-Lower Ordovician (pre-Sardic) sequence from the Upper Ordovician-lower Carboniferous (post-Sardic) sequence (Loi et al., 2023). The Upper Ordovician begins with sediments documenting a continental facies passing above to a storm-dominated terrigenous platform facies. The basal Monte Argentu Formation (200–600 m of conglomerates, sandstones and coarse siltstones; Laske et al., 1994) is conformably capped by the 200–280 m-thick Monte Orri and Portixeddu formations (siltstones, argillites and silty sandstones attributed to the Sandbian-early Katian). The following Domusnovas Formation (90 m-thick; late Katian) is constituted in succession by the Maciurru Member (quartz-arenites and quartz microconglomerates) and the following Punta S'Argiola Member (marly limestones, marly shales and limestones). The latter has provided rich brachiopod and trilobite faunas and the conodont association described below. According to Loi et al. (2023), the Punta S'Argiola Member of the Domusnovas Formation is associated to a high degree of sedimentary condensation, testified by a carbonation of the seabed. The Rio San Marco Formation (230 m of basal siltstones, shales, and interbedded conglomerates, passing to sandstones and shales and topped by glacio-marine deposits) is attributed to the Hirnantian (Leone et al., 1991). Silurian-Devonian sediments follow in conformity, initially with typical organic carbon-rich black shales and later with organic carbon-rich limestones in SW Sardinia (Barca et al., 1992; Ferretti and Serpagli, 1996; Gnoli et al., 1990; Negri et al., 2009a, 2009b). Pelagic nodular limestones are exposed in SE Sardinia (*e.g.*, Corradini et al., 1998; Ferretti and Serpagli, 1996).

Investigated material comes from the Cannamenda outcrop, located about 2.5 km from the Bacu Abis village. Ferretti and Serpagli (1991,

1998) and Ferretti et al. (1998a) documented an abundant and moderately diverse conodont fauna from a thin fossiliferous horizon (4–4.5 cm) of the Punta S'Argiola Member, there exposed as sparse limestone chunks in the field due to the strong tectonic activity affecting the area. Conodonts are dominant in the finer-grained pinkish-grey samples. Conodont elements are not well preserved and often broken, having a Colour Alteration Index (CAI) (Epstein et al., 1977) of 5. Fourteen species belonging to 13 genera were there recognized and assigned to the Late Ordovician *Amorphognathus ordovicicus* Zone.

2.2. Carnic Alps

The Carnic Alps (locality 2 in Fig. 1) expose at the geographic border between southern Austria and northern Italy one of the most complete and well-studied Paleozoic successions of the world, ranging in age from the ?Cambrian-Early Ordovician to the Late Permian. The continuity of the successions, combined with the excellent preservation and abundance of the fossil material, have allowed a precise integrated biostratigraphic constraint. Thirty-six lithostratigraphic units have been recently formally introduced in the so-called Pre-Variscan sequence (rocks up to the Lower Pennsylvanian) by a working group of Austrian and Italian scientists (Corradini and Suttner, 2015).

As regards the Ordovician, terrigenous successions of the Early and Middle Ordovician are followed by siltstones and fossiliferous limestones of Late Ordovician age, punctuated by ignimbrites or submarine lava outflows in the Middle-Late Ordovician, suggesting a shallow to moderately deep marine environment (Ferretti et al., 2023a).

The Uqua Valley and Valbertad area (Italy), situated in the vicinity of the Rifugio Nordio in the upper part of the Uqua Valley north of the village of Ugovizza, represent an historical location discovered by Stache (1884). There, the Ordovician exposes the Valbertad Formation (siltstones), followed by the Uqua Formation (calcareous sandstones and limestones) and the Plöcken Formation (sandstones), the latter attributed to the Hirnantian (Ferretti et al., 2023a). The Uqua Formation is a 1.5 to 9 m-thick unit easily recognizable in the field as a flaser-type limestone with siltstone intercalations near the top (Schönlaub and Ferretti, 2015). The unit has been associated to a calm offshore environment in an open sea bordering the North Gondwana continental plate (Ferretti et al., 2023a).

Together with conodonts (see below), acritarchs, brachiopods, cephalopods, chitinozoans, echinoderms, foraminiferans, gastropods, ostracods, sponge spicules, trilobites and trace fossils have been reported. Ordovician conodont investigation in all southern Europe started just from this area, thanks to the pioneer papers of Serpagli and Greco (1965a, 1965b) followed by the extensive monograph of Serpagli (1967) from the Rifugio Nordio and Monte Zermula sites on the Italian side of the Carnic Alps, describing a superb rich and well-diversified conodont association. Remarkably, conodont elements, still reported in form-taxonomy as used at that time, were illustrated only by hand-made drawings. Following studies on the Late Ordovician conodont faunas were sourced by other outcrops or slightly younger horizons (Bagnoli et al., 1998, 2017; Corriga et al., 2021; Ferretti et al., 2023a; Ferretti and Schönlaub, 2001; Flajs and Schönlaub, 1976; Manara and Vai, 1970; Schönlaub, 1971; Schönlaub et al., 2017; Vai and Spalletta, 1980), that confirmed the attribution of the conodont association from the Uqua Formation to the Late Ordovician *Amorphognathus ordovicicus* Zone and assigned CAI values ranging from 5 to 6.

3. Materials and methods

3.1. Analyzed material

Investigated material was chosen from the two localities of Cannamenda (SW Sardinia) and Monte Zermula (Carnic Alps) in order to share the same age (Late Ordovician, *Amorphognathus ordovicicus* Zone) and the same *Hamarodus europaeus* (now *brevirameus*) - *Dapsilodus mutatus* - *Scabbardella altipes* (HDS) conodont biofacies (Ferretti and Serpagli, 1998; Sweet and Bergström, 1984). The HDS biofacies, together with the *Amorphognathus* - *Plectodina* biofacies (British middle-upper Katian faunas from Wales and England; Bergström and Ferretti, 2015; Ferretti et al., 2014) occupied medium to low-latitudes, being the *Sagittodontina robusta* - *Scabbardella altipes* biofacies typical of the high-latitude, relatively cold waters near the pole (Sweet and Bergström, 1984).

Material was first examined under optical microscopy with a Zeiss Stemi SV 11 binocular microscope (magnification 25-100×) in order to select taxa and later characterized under SEM to define smooth and euhedral crystal areas to be processed to further investigation. The illustrated specimens (Fig. 2) are kept in the Type Collection of the Department of Chemical and Geological Sciences, University of Modena and Reggio Emilia, Modena, Italy under the Repository Numbers IPUM 35040–35047. A total of 23 conodont elements was selected. Twelve specimens were provided by the Cannamenda fauna: *Hamarodus brevirameus* (two Pa elements; one Pb element, Fig. 2.3; one M element, Fig. 2.6; two Sc elements, one illustrated in Fig. 2.7; one Sd element); *Dapsilodus mutatus* (one element; Fig. 2.8); *Panderodus gracilis* (one element); *Plectodina sp.* (one Sc element); *Scabbardella altipes* (two elements). A recent reorganization of the Paleontological Collections of the University of Modena and Reggio Emilia allowed to rediscover the original residues of Serpagli (1967). A new picking of the material from the classic locality Monte Zermula provided a small conodont fauna, from which we selected, and herein illustrated for the first time with SEM micrographs, eleven conodont elements, including both cosmopolitan and restricted/endemic taxa: *Hamarodus brevirameus* (one Sc element); *Plectodina alpina* (one Pa element, Fig. 2.5; one Pb element, one Sa element, Fig. 2.4); *Scabbardella altipes* (two elements); *Nordiodus italicus* (two Pa elements; two Pb elements, Figs. 2.1 and 2.2; one Sa element); *Amorphognathus sp.* (one Sc element).

3.2. Instruments and analytical methods

Electron microscopy data were collected using the Scanning Electron Microscope (SEM) JEOL JSM–6010PLUS/LA InTouchScope at the Department of Chemical and Geological Sciences of the University of Modena and Reggio Emilia. Scanning Electron Microscope measurements were performed in high vacuum with an accelerating voltage between 5 and 20 keV. Selected specimens were mounted on aluminum stubs previously covered with carbon-conductive adhesive tape. Rare Earth Elements and other trace elements were measured using the ICP-MS X Series II (Thermo Fisher Scientific) equipped with the 213 nm laser ablation device UP-213 (New Wave Research) at the Scientific Instruments Facility (CIGS) of the University of Modena and Reggio Emilia.

As is well known and extensively documented in the literature, the tuning of experimental parameters for laser ablation is critical. The experimental conditions adopted in this research substantially parallel those recently employed by our research-team (Ferretti et al., 2023b; Malferrari et al., 2019; Medici et al., 2021; Nardelli et al., 2016). In brief, the instrument was firstly tuned using NIST SRM 610 and NIST SRM 612 by measuring, under optimized working conditions, the signal intensities of U and Th (U/Th *vs* U). A tablet was then prepared with NIST 1400 (bone ash) standard and, using NIST SRM 610 and NIST SRM 612 as calibration standards, the ablation parameters were modulated until, for the NIST 1400 tablet, the concentrations of selected trace element were close to those certified. The optimized ablation parameters were then applied to standards (NIST SRM 610 and NIST SRM 612) and samples. The main difference with previous studies concerns the dimension of the ablation line, here optimized to 30 μm, to perform the measurement even on the small portions of the euhedral crystals. It is worth mentioning, however, that the specific objective of this research was to evaluate differences in HFSE concentrations on euhedral crystals and smooth portions at the conodont element, not to obtain absolute concentrations to compare, for example, with specimens from other

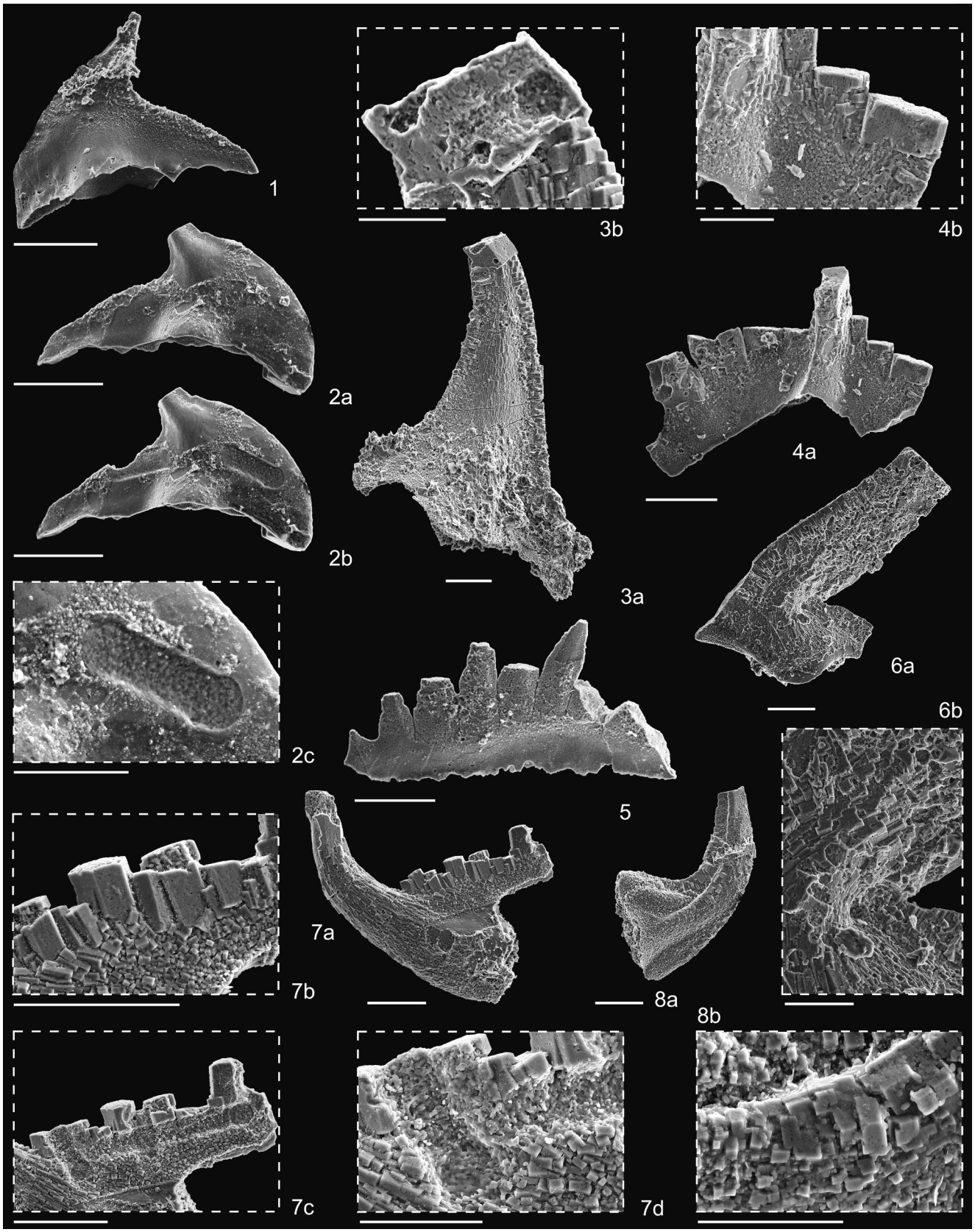

(caption on next page)

Fig. 2. SEM micrographs of selected conodonts investigated in this study. Late Ordovician, *Amorphognathus ordovicicus* Zone.
1, *Nordiodus italicus* Serpagli, 1967, Pb element, lateral view of specimen MZ 56, IPUM 35040. Carnic Alps, sample Monte Zermula 19AII.
2, *Nordiodus italicus* Serpagli, 1967, Pb element, lateral view of specimen MZ 63, IPUM 35041, before (a) and after (b) the application of laser ablation; two "ablation scars" are visible on the surface of the specimen. Inset 2c details the right ablated line of 2b. Carnic Alps, sample Monte Zermula 19AII.
3, *Hamarodus brevirameus* (Walliser, 1964), Pb element, lateral view (a) of specimen CDA 39, IPUM 35042, with detail (b) of the ablated line in the summit euhedral crystal grown at the cusp tip. Sardinia, sample Cannamenda rosa.
4, *Plectodina alpina* (Serpagli, 1967), Sa element, posterior view (a) of specimen MZ 23, IPUM 35043, with detail (b) of the euhedral crystals grown at the denticle tips. Tiny apatite crystals are present all over the surface of the element. Carnic Alps, sample Monte Zermula 19AII.
5, *Plectodina alpina* (Serpagli, 1967), Pa element, lateral view of specimen MZ 51, IPUM 35044, exposing a smooth surface running along the base of the element. Carnic Alps, sample Monte Zermula 19AI.
6, *Hamarodus brevirameus* (Walliser, 1964), M element, lateral view (a) of specimen CDA 18, IPUM 35045, with detail (b) of the oriented apatite euhedral crystals covering the element surface. Sardinia, sample Cannamenda rosa.
7, *Hamarodus brevirameus* (Walliser, 1964), Sc element, lateral view (a) of specimen CDA 42, IPUM 35046, with detail (b) of the euhedral crystals replacing denticles of the posterior process. Small crystals are covering the entire surface of the element. Ablated lines along the posterior process and along a single denticle of the process are visible in frame (c), with detail of the latter in (d). Sardinia, sample Cannamenda rosa.
8, *Dapsilodus mutatus* (Branson and Mehl, 1933), lateral view (a) of specimen CDA 34, IPUM 35047, fully covered by sub-equal apatite crystals detailed in inset (d). Sardinia, sample Cannamenda rosa.
Scale bar corresponds to 100 μm for all frames except for 2c, 3b, 4b, 6b, 7d and 8b where it corresponds to 50 μm.

outcrops.

4. Results

4.1. Microtextures

Ferretti et al. (2017) discriminated three microtextural patterns in the authigenic apatite crystal overgrowth on the external surfaces of conodont elements from the Late Ordovician of Normandy, northern France. Long prismatic crystals (up to 20 μm in length) define the large columnar crystal microtexture, with crystals that often replace cusp tips or process denticles. Smaller isometric crystals, up to 10 μm in length, characterize the blocky crystal microtexture as a sort of "sugar-grains sprinkled over the conodont surface" (Ferretti et al., 2017, p. 4–5). Crystals arranged as circular rims, often bordering areas with no visible crystal pattern, were associated to the web-like crystal microtexture, common also on platform elements.

All the three types of crystal microtextures (large columnar, blocky and web-like) have been recognized in our material. The former two types have been selected for detecting the HFSE signature in order to amplify differences between euhedral crystals and smooth areas of the conodont elements.

4.2. HFSE signature

A list of significant diagenetic-related relationships (*e.g.*, Chen et al., 2015; Ferretti et al., 2023b; Li et al., 2017; Liao et al., 2019; Liu et al., 2008; Medici et al., 2021; Trotter et al., 2016; Zhang et al., 2016, see also Introduction) among the HFSE of the investigated material is given in Annex-1A whereas raw data are reported in Annex-1B (both supplied as Supplementary Online Material). All specimens, regardless of geographical provenance and type of investigated spot (euhedral crystals or smooth surface), are characterized by substantial enrichment of MREE and, to a lesser extent, HREE (Fig. 3). This trend is also evidenced by the linear distribution of Y with respect to La, Nd and Yb (Fig. 4) considered as representative of LREE, MREE and HREE, respectively.

One REE often investigated in literature is Ce, since it can be oxidized with the formation of Ce(IV) compounds that are poorly soluble or easily adsorbed on suspended particulate (Sholkovitz and Shen, 1995). This event may lead to a negative Ce anomaly (*i.e.*, Ce/Ce* <1.0) in seawater, possibly enhanced also by an alkaline pH (de Baar et al., 1988; Liu et al., 1988). In contrast, in anoxic environments Ce(III) behaves similarly to the other REE, not inducing significant anomalies (*i.e.*, Ce/Ce* ~1.0). Therefore, Ce anomalies are usually assumed as a paleoenvironmental indicator (see for example Zhang and Shields, 2022 for a recent review). Sometimes the Ce anomaly is only apparent being due to an anomalous content of adjacent REE (*i.e.*, La and Pr); for this reason, the Pr/Pr* *vs*

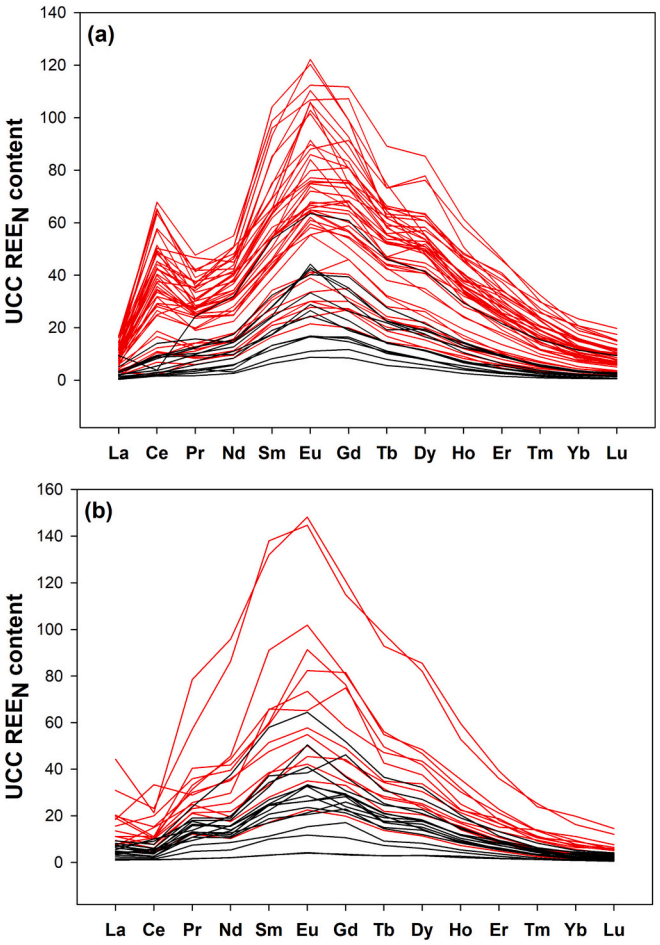

Fig. 3. Upper continental crust (UCC) normalized (McLennan, 2001) REE abundance patterns for conodonts from Sardinia (a) and the Carnic Alps (b). The red and black lines denote measurements made on portions of euhedral crystals or on smooth surfaces, respectively (see Fig. 2). (For interpretation of the references to colour in this figure legend, the reader is referred to the web version of this article.)

Ce/Ce* cross-plots, where Pr/Pr* = $2Pr_N/(CeN + Nd_N)$ and Ce/Ce* = $3Ce_N/(2La_N + Nd_N)$ with N indicating normalized values, are considered a better tool to estimate true Ce anomalies (Bau and Dulski, 1996; Chen et al., 2015; Kowal-Linka et al., 2014; Zhang et al., 2016). The Ce/Ce* *vs* Pr/Pr* cross-plot (Fig. 5) shows that samples from the Carnic Alps exhibit a moderate negative Ce anomaly, while samples from Sardinia

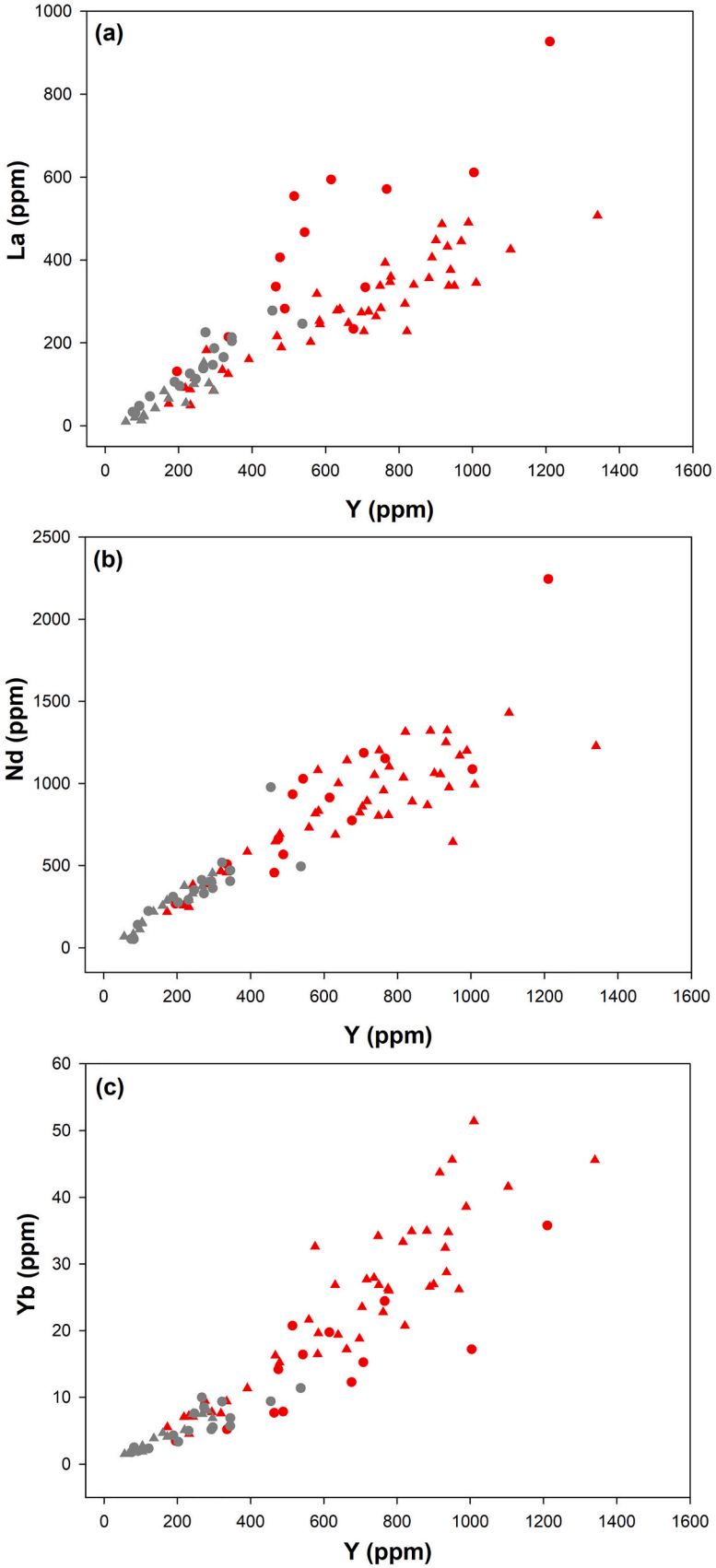

Fig. 4. Cross-plots of La (a), Nd (b) and Yb (c) *vs* Y. Legend: samples from Sardinia (triangles) and Carnic Alps (circles); measurements on euhedral crystals (red symbols) and on smooth surfaces (grey symbols). (For interpretation of the references to colour in this figure legend, the reader is referred to the web version of this article.)

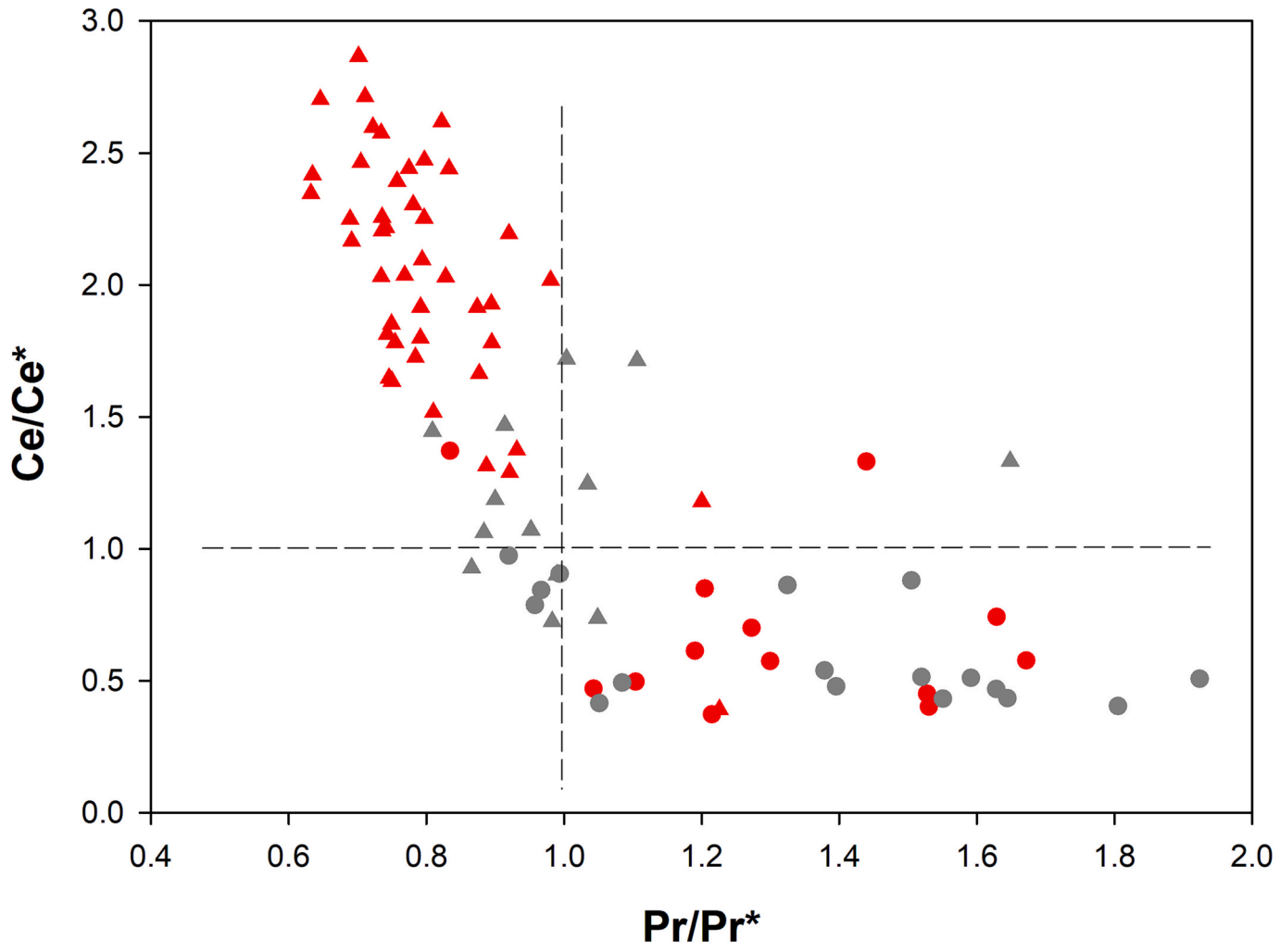

Fig. 5. McLennan (2001) normalized cross-plot of Ce/Ce* *vs* Pr/Pr*. Adapted from Kowal-Linka et al. (2014). Symbols like in Fig. 4.

reveal a moderate to strongly positive anomaly, in both cases regardless of whether measurements are taken on euhedral crystals or on the smooth surfaces.

One method to assess the influence of siliciclastic detritus on REE and HFSE composition is to examine the relationship between the concentrations of Th and ΣREE (or log[ΣREE] to better emphasize the dependence at increasing values as here plotted in Fig. 6a) (*e.g.*, Chen et al., 2015; Zhang et al., 2016). Euhedral crystals are generally enriched in ΣREE with respect to smooth surfaces (Annex-1), without showing, however, any significant correlation with Th. On the other hand, when considering the cross-plot La + Th *vs* log[ΣREE] (Fig. 6b), thus introducing also the contribution of a light REE, a positive correlation clearly emerges. Another approach to evaluate detrital siliciclastic influence is through the Y/Ho ratio, which usually ranges between 20 and 30 in samples where REE content is boosted from lithogenic source (Chen et al., 2015; Zhao et al., 2013), whereas it is higher than 60 when the hydrogen signature (marine water) prevails since Ho in seawater is preferentially adsorbed onto marine particulates (McLennan, 2001; Webb and Kamber, 2000). In conodont elements both from Sardinia and the Carnic Alps the Y/Ho ratios mainly range between 22 and 38, with a marked decrease when referring to measurements on euhedral crystals (Fig. 6c).

5. Discussion

Conodonts are getting more and more significance in recognizing geochemical signatures of past oceans and seas. Bioapatite acts in fact as an important archive of sea/pore water chemistry and its reliability is being tested with several paleoceanographic/paleoclimatic proxies. The application of HFSE (and REE) is certainly one of the most recent approach, but still in an embryonal stage for a better regional or global understanding of the ocean/sea dynamics. Normalized distributions, anomalies, and correlations between REE and other elements (major or trace) have long been widely used for paleoceanographic reconstructions, and defining their origin and correlation with diagenetic events has always represented an intriguing challenge.

All the samples analyzed in this research undoubtedly show a considerable diagenetic imprint although more evident from measurements made on euhedral crystals rather than on the smooth surfaces of the conodont elements. The enrichment in MREE (Fig. 3), an event frequently documented in the literature (*e.g.*, Bright et al., 2009; Grandjean et al., 1987; Grandjean-Lécuyer et al., 1993; Kidder et al., 2003; Lécuyer et al., 2004; Lumiste et al., 2023; Zhao et al., 2013) although not yet explained with certainty, is significantly more pronounced for euhedral crystals rather than for smooth surfaces. The enrichment in MREE is usually related to selective adsorption of LREE and HREE by Mn and Fe oxides and hydroxides, leaving MREE in pore waters (Haley et al., 2004; Prakash et al., 2012; Soyol-Erdene and Huh, 2013). The enrichment observed for the euhedral crystals, which reasonably form during burial and diagenesis, in addition to confirming this hypothesis, would also suggest that the crystals form in the early stages of diagenesis when porosity water (enriched in MREE) and

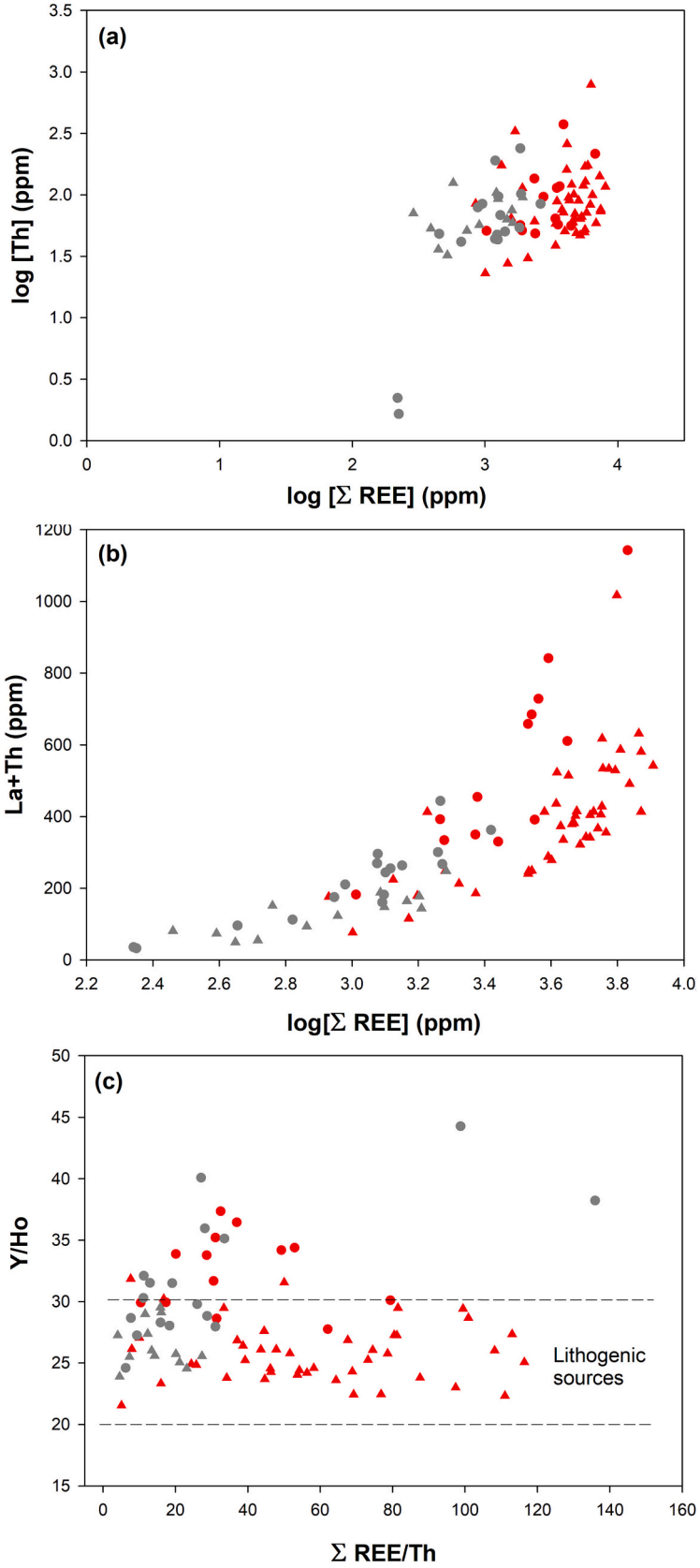

Fig. 6. Cross-plots of log[Th] *vs* log[ΣREE] (a), La + Th *vs* log[ΣREE] (b), and Y/Ho *vs* ΣREE/Th (c). Symbols like in Fig. 4. The field between dashed lines in Fig. 6c is representative of lithogenic sources.

microcavities allow euhedral crystal growth. The diagenetic sources of conodonts REE can also be corroborated by the high La/Yb ratios observed for all samples (median 13.85, mean value 17.45, standard deviation 8.83 - see Annex-1). Such enrichment of LREE may develop as a result of fractionation related to the adsorption/desorption of REE by clay minerals (Yan et al., 1999). The occurrence of two perceptibly distinct REE distributions for euhedral crystals and smooth surfaces, well-marked by plots of Figs. 4 and 6, suggests that the imprint defined by the elements resulting from the leaching of the detrital component should be considered more relevant for euhedral crystals regardless of the geographic area of provenience. In fact, crystals are generally characterized by higher values of ΣREE (Figs. 6a and 6b). Low values of ΣREE and Th suggest a non-detritic derivation, while higher values of ΣREE but lower values of ΣREE/Th reflect a more rapid uptake of Th than REE during diagenesis. It is, however, relevant to observe a direct correlation when considering the relationship La + Th *vs* log[ΣREE] (Fig. 6b). This behavior is possibly due to "primary" low-Th and low-ΣREE components (Chen et al., 2015), which could have been subsequently overprinted by a progressive diagenetic imprint that progressively removed LREE not only from the sediment, but also from the conodont element bioapatite. This hypothesis matches with the Ce anomalies, which do not correlate with the measurement point (euhedral crystals or the smooth surfaces), keeping the same oxidation state (in other words, Ce follows the same fate as La as shown in Fig. 7).

This assumption would arise from the need to consider conodont elements as modified as a whole, since there are not data from literature which differentiate REE contents with respect to the crystalline type of surface of the conodonts. In fact, systems such as those studied by Chen et al. (2015) and Zhang et al. (2016), which showed higher REE contents of conodonts with respect to sediments, did not distinguish between smooth surfaces and neoformed crystals (Liu et al., 2008), and their results should represent a chemical mean of the conodont surfaces. On the other hand, our data point two different surface chemistries of conodont elements: one could result from purely diagenetic transformations, represented by REE-enriched euhedral crystals; the other, also diagenetic, but better reflecting the original biomineralized tissue represented by the smooth surfaces. In other words, the particular partition equilibrium between the two apatitic components seems to highlight the different nature of euhedral crystals and smoothed surfaces, where the latter are what still remain of the conodont pristine bioapatite after diagenesis. Besides, it seems safe to assume that a removing process from smooth surfaces to crystals would have led to a chemical equilibrium with similar REE contents between the two bioapatites, due to their same crystal structure (Ferretti et al., 2017).

6. Conclusion

Through this research, differences with respect to trace element contents measured in conodont elements from the Late Ordovician of Sardinia and the Carnic Alps (Italy) are detected; measurements were carried out both on smooth surfaces and on euhedral crystals grown on the conodont element surfaces. The experimental results indicated that

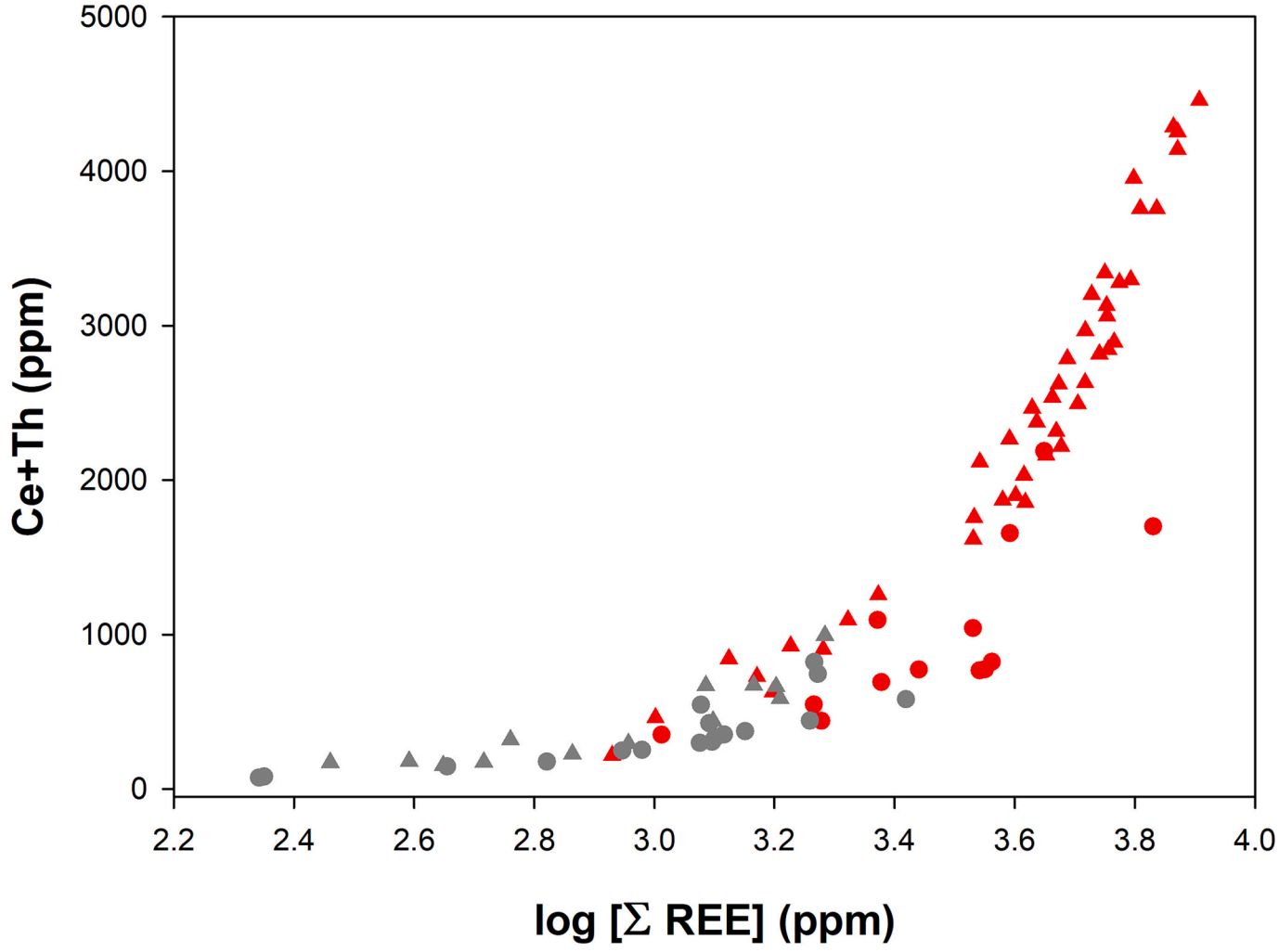

Fig. 7. Cross-plots of Ce + Th *vs* log[ΣREE]. Symbols like in Fig. 4.

the crystals are significantly more enriched in MREE and, subordinately, HREE. The positive correlations between La + Th *vs* log[ΣREE] and Ce + Th *vs* log[ΣREE] could support the hypothesis that euhedral crystals during growth also progressively removed part of the light REE from the conodont bioapatite, depleting the LREE signature. Anyway, it cannot be excluded that the euhedral crystals, with higher REE contents, represented the true products of diagenetic processes, whereas the smooth surfaces, with lower REE contents, are what is closest to the pristine element, although the latter has also been modified by diagenesis. This work and these hypotheses highlight the obligation to study bioapatite geochemical systems through accurate procedures and precise instrumental techniques. Moreover, these results suggest caution in any use of REE contents of conodont elements as paleo-proxy source.

Declaration of Competing Interest

The authors declare that they have no known competing financial interests or personal relationships that could have appeared to influence the work reported in this paper.

Data availability

Data are provided as Supplementary Material

Acknowledgements

The Authors kindly acknowledge the journal Editor for the skilled editorial guidance during manuscript preparation. Suggestions provided by Prof. Živilė Žigaitė and two anonymous Reviewers are acknowledged. We are grateful as well to the Scientific Instruments Facility, CIGS (University of Modena and Reggio Emilia), and especially to Daniela Manzini and Lisa Lancellotti for LA-ICPMS expertise and to Simona Bigi and Simona Marchetti Dori (Department of Chemical and Geological Sciences, University of Modena and Reggio Emilia) for skilled assistance at the SEM.

This research was undertaken within the framework and with the financial support of the Italian Ministry of University and Research, project P2022K9BE8, PRIN-PNRR 2022 "OCEANS – impacts Of aCidification on past biodivErsity: insights from mAriNe vertebrateS" (to AF, Resp. Manuel Rigo) and project 2022MAM9ZB, PRIN-2022 "BIOVERTICES (BIOdiversity of VERTebrates In the CEnozoic Sea)" (to AF and LM, Resp. Alberto Collareta). This paper is a contribution to the IGCP Project n. 735 "Rocks and the Rise of Ordovician Life: Filling knowledge gaps in the Early Palaeozoic Biodiversification".

Appendix A. Supplementary data

Supplementary data to this article can be found online at https://doi.org/10.1016/j.marmicro.2023.102308.

References

Armstrong, H.A., Pearson, D.G., Griselin, M., 2001. Thermal effects on rare earth element and strontium isotope chemistry in single conodont elements. Geochim. Cosmochim. Acta 65, 435–441. https://doi.org/10.1016/S0016-7037(00)00548-2.

de Baar, H.J.W., German, C.R., Elderfield, H., van Gaans, P., 1988. Rare earth element distributions in anoxic waters of the Cariaco Trench. Geochim. Cosmochim. Acta 52, 1203–1219. https://doi.org/10.1016/0016-7037(88)90275-X.

Bagnoli, G., Ferretti, A., Serpagli, E., Vai, G.B., 1998. Late Ordovician conodonts from the Valbertad section (Carnic Alps). Giorn. Geol. 60 (Spec. Issue), 138–149.

Bagnoli, G., Ferretti, A., Simonetto, L., Corradini, C., 2017. Upper Ordovician conodonts in the Valbertad section. Ber. Inst. Erdwissenschaften K.-F.-Univ. Graz 23, 228–231.

Barca, S., Ferretti, A., Massa, P., Serpagli, E., 1992. The Hercynian Arburese tectonic unit of SW Sardinia new stratigraphic and structural data. Riv. It. Paleont. Strat. 98, 119–136.

Bau, M., Dulski, P., 1996. Distribution of yttrium and rare-earth elements in the Penge and Kuruman iron-formations, Transvaal Supergroup, South Africa. Precambrian Res. 79, 37–55. https://doi.org/10.1016/0301-9268(95)00087-9.

Bergström, S.M., Ferretti, A., 2015. Conodonts in the Upper Ordovician Keisley Limestone of northern England: taxonomy, biostratigraphical significance and biogeographical relationships. Pap. Palaeontol. 1, 1–32. https://doi.org/10.1002/spp2.1003.

Branson, E.B., Mehl, M.G., 1933. Conodonts from the Maquoketa-Thebes (Upper Ordovician) of Missouri. University of Missouri Studies 8, 121–132.

Brigatti, M.F., Malferrari, D., Medici, L., Ottolini, L., Poppi, L., 2004. Crystal chemistry of apatites from the Tapira carbonatite complex, Brazil. Eur. J. Mineral. 16, 677–685. https://doi.org/10.1127/0935-1221/2004/0016-0677.

Bright, C.A., Cruse, A.M., Lyons, T.W., MacLeod, K.G., Glascock, M.D., Ethington, R.L., 2009. Seawater rare-earth element patterns preserved in apatite of Pennsylvanian conodonts? Geochim. Cosmochim. Acta 73, 1609–1624. https://doi.org/10.1016/j.gca.2008.12.014.

Chen, J., Algeo, T.J., Zhao, L., Chen, Z.-Q., Cao, L., Zhang, L., Li, Y., 2015. Diagenetic uptake of rare earth elements by bioapatite, with an example from Lower Triassic conodonts of South China. Earth Sci. Rev. 149, 181–202. https://doi.org/10.1016/j.earscirev.2015.01.013.

Corradini, C., Suttner, T.J. (Eds.), 2015. The Pre-Variscan sequence of the Carnic Alps (Austria and Italy). Abh. Geol. Bundesanst. 69, 1–158.

Corradini, C., Ferretti, A., Serpagli, E., Barca, S., 1998. The Ludlow-Pridoli section Genna Ciuerciu, west of Silius. Giorn. Geol. 60, 112–118.

Corriga, M.G., Corradini, C., Pondrelli, M., Schönlaub, H.-P., Nozzi, L., Todesco, R., Ferretti, A., 2021. Uppermost Ordovician to lowermost Devonian conodonts from the Valentintörl section and comments on the post Hirnantian hiatus in the Carnic Alps. Newsl. Stratigr. 54, 183–207. https://doi.org/10.1127/nos/2020/0614.

Epstein, A.G., Epstein, J.B., Harris, L.D., 1977. Conodont color alteration-an index to organic metamorphism. Geol. Surv. Prof. Pap. 995, 1–27.

Fadel, A., Žigaitė, Ž., Blom, H., Perez-Huerta, A., Jeffries, T., Märss, T., Ahlberg, P.E., 2015. Palaeoenvironmental signatures revealed from rare earth element (REE) compositions of vertebrate microremains of the Vesiku Bone Bed (Homerian, Wenlock), Saaremaa Island, Estonia. Eston. J. Earth Sci. 64 (1), 36–41. https://doi.org/10.3176/earth.2015.07.

Ferretti, A., Schönlaub, H.P., 2001. New conodont faunas from the Late Ordovician of the Central Carnic Alps, Austria. Boll. Soc. Paleontol. Ital. 40, 3–15.

Ferretti, A., Serpagli, E., 1991. First record of Ordovician conodonts from southwestern Sardinia. Riv. It. Paleont. Strat. 97, 27–34.

Ferretti, A., Serpagli, E., 1996. Geological outline, community sequence and paleoecology of the Silurian of Sardinia. Riv. It. Paleont. Strat. 102, 353–362.

Ferretti, A., Serpagli, E., 1998. Late Ordovician conodont faunas from southern Sardinia, Italy: biostratigraphic and paleogeographic implications. Boll. Soc. Paleontol. Ital. 37, 215–236.

Ferretti, A., Serpagli, E., Hammann, W., Leone, F., 1998a. Conodonts and biofacies from the late Ordovician of Cannamenda (Bacu Abis). Giorn. Geol. 60 (Spec. Issue), 178–187.

Ferretti, A., Bergström, S.M., Barnes, C.R., 2014. Katian (Upper Ordovician) conodonts from Wales. Palaeontology 57, 801–831. https://doi.org/10.1111/pala.12089.

Ferretti, A., Malferrari, D., Medici, L., Savioli, 2017. Diagenesis does not invent anything new: Precise replication of conodont structures by secondary apatite. Sci. Rep. 7, 1624. https://doi.org/10.1038/s41598-017-01694-4.

Ferretti, A., Medici, L., Savioli, M., Mascia, M.T., Malferrari, D., 2021. Dead, fossil or alive: Bioapatite diagenesis and fossilization. Palaeogeogr. Palaeoclimatol. Palaeoecol. 579, 110608 https://doi.org/10.1016/j.palaeo.2021.110608.

Ferretti, A., Schönlaub, H.P., Sachanski, V., Bagnoli, G., Serpagli, E., Vai, G.B., Yanev, S., Radonjić, M., Balica, C., Bianchini, L., Colmenar, J., Gutiérrez-Marco, J.C., 2023a. A global view on the Ordovician stratigraphy of South-Eastern Europe. In: Harper, D. A.T., Lefebvre, B., Percival, I., Servais, T. (Eds.), A Global Synthesis of the Ordovician System Part 1. Geol. Soc. Spec. Publ., vol. 532, pp. 465–499. https://doi.org/10.1144/SP532-2022-174.

Ferretti, A., Corradini, C., Fakir, S., Malferrari, D., Medici, L., 2023b. To be or not to be a conodont. The controversial story of *Pseudooneotodus* and *Eurytholia*. Mar. Micropaleontol. 182, 102258 https://doi.org/10.1016/j.marmicro.2023.102258.

Flajs, G., Schönlaub, H.P., 1976. Die biostratigraphische Gliederung des Altpaläozoikums am Polster bei Eisenerz (Nördliche Grauwackenzone, Osterreich). Verh. Geol. Bundesanst. 2, 257–303.

Gnoli, M., Kříž, F., Leone, F., Olivieri, F., Serpagli, E., Storch, P., 1990. Lithostratigraphic units and biostratigraphy of the Silurian and Early Devonian of Southwest Sardinia. Boll. Soc. Paleontol. Ital. 23, 221–238.

Grandjean, P., Cappetta, H., Michard, A., Albare'de, F., 1987. The assessment of REE patterns and 143Nd/144Nd ratios in fish remains. Earth Planet. Sci. Lett. 84, 181–196. https://doi.org/10.1016/0012-821X(87)90084-7.

Grandjean-Lécuyer, P., Feist, R., Albarède, F., 1993. Rare earth elements in old biogenic apatites. Geochim. Cosmochim. Acta 57, 2507–2514. https://doi.org/10.1016/0016-7037(93)90413-Q.

Haley, B.A., Klinkhammer, G.P., McManus, J., 2004. Rare earth elements in pore waters of marine sediments. Geochim. Cosmochim. Acta 68, 1265–1279. https://doi.org/10.1016/j.gca.2003.09.012.

Herwartz, D., Tütken, T., Jochum, K.P., Sander, P.M., 2013. Rare earth element systematics of fossil bone revealed by LA-ICPMS analysis. Geochim. Cosmochim. Acta 103, 161–183. https://doi.org/10.1016/j.gca.2012.10.038.

Holser, W.T., 1997. Evaluation of the application of rare-earth elements to paleoceanography. Palaeogeogr. Palaeoclimatol. Palaeoecol. 132, 309–323. https://doi.org/10.1016/S0031-0182(97)00069-2.

Keenan, S.W., Engel, A.S., 2017. Early diagenesis and recrystallization of bone. Geochim. Cosmochim. Acta 196, 209–223. https://doi.org/10.1016/j.gca.2016.09.033.

Keenan, S.W., Engel, A.S., Roy, A., Lisa Bovenkamp-Langlois, G., 2015. Evaluating the consequences of diagenesis and fossilization on bioapatite lattice structure and composition. Chem. Geol. 413, 18–27. https://doi.org/10.1016/j.chemgeo.2015.08.005.

Kidder, D.L., Krishnaswamy, R., Mapes, R.H., 2003. Elemental mobility in phosphatic shales during concretion growth and implications for provenance analysis. Chem. Geol. 198, 335–353. https://doi.org/10.1016/S0009-2541(03)00036-6.
Kim, J.-H., Torres, M.E., Haley, B.A., Kastner, M., Pohlman, J.W., Riedel, M., Lee, Y.-J., 2012. The effect of diagenesis and fluid migration on rare earth element distribution in pore fluids of the northern Cascadia accretionary margin. Chem. Geol. 291, 152–165. https://doi.org/10.1016/j.chemgeo.2011.10.010.
Kocsis, L., Trueman, C.N., Palmer, M.R., 2010. Protracted diagenetic alteration of REE contents in fossil bioapatites: Direct evidence from Lu-Hf isotope systematics. Geochim. Cosmochim. Acta 74, 6077–6092. https://doi.org/10.1016/j.gca.2010.08.007.
Kowal-Linka, M., Jochum, K.P., Surmik, D., 2014. LA-ICP-MS analysis of rare earth elements in marine reptile bones from the Middle Triassic bonebed (Upper Silesia, S Poland): Impact of long-lasting diagenesis, and factors controlling the uptake. Chem. Geol. 363, 213–228. https://doi.org/10.1016/j.chemgeo.2013.10.038.
Laske, R., Bechstädt, T., Boni, M., 1994. The post-Sardic Ordovician series. In: Bechstädt, T., Boni, M. (Eds.), Sedimentological, Stratigraphical and Ore Deposits Field Guide of the Autochtonous Cambro-Ordovician of Southeastern Sardinia. Memorie Descrittive della Carta Geologica d'Italia, vol. 48, pp. 115–146.
Lécuyer, C., Bogey, C., Garcia, J.-P., Grandjean, P., Barrat, J.-A., Floquet, M., Bardet, N., Pereda-Superbiola, X., 2003. Stable isotope composition and rare earth element content of vertebrate remains from the Late Cretaceous of northern Spain (Laño): did the environmental record survive? Palaeogeogr. Palaeoclimatol. Palaeoecol. 193, 457–471. https://doi.org/10.1016/S0031-0182(03)00261-X.
Lécuyer, C., Reynard, B., Grandjean, P., 2004. Rare earth element evolution of Phanerozoic seawater recorded in biogenic apatites. Chem. Geol. 204, 63–102. https://doi.org/10.1016/j.chemgeo.2003.11.003.
Leone, F., Hammann, W., Laske, R., Serpagli, E., Villas, E., 1991. Lithostratigraphic units and biostratigraphy of the post-sardic Ordovician sequence in South-West Sardinia. Boll. Soc. Paleontol. Ital. 30, 201–235.
Li, Y., Zhao, L., Chen, Z.-Q., Algeo, T.J., Cao, L., Wang, X., 2017. Oceanic environmental changes on a shallow carbonate platform (Yangou, Jiangxi Province, South China) during the Permian-Triassic transition: Evidence from rare earth elements in conodont bioapatite. Palaeogeogr. Palaeoclimatol. Palaeoecol. 486, 6–16. https://doi.org/10.1016/j.palaeo.2017.02.035.
Liao, J., Sun, X., Li, D., Sa, R., Lu, Y., Lin, Z., Xu, L., Zhan, R., Pan, Y., Xu, H., 2019. New insights into nanostructure and geochemistry of bioapatite in REE-rich deep-sea sediments: LA-ICP-MS, TEM, and Z-contrast imaging studies. Chem. Geol. 512, 58–68. https://doi.org/10.1016/j.chemgeo.2019.02.039.
Liu, Y., Hu, Z., Gao, S., Günther, D., Xu, J., Gao, C., Chen, H., 2008. *In situ* analysis of major and trace elements of anhydrous minerals by LA-ICP-MS without applying an internal standard. Chem. Geol. 257, 34–43. https://doi.org/10.1016/j.chemgeo.2008.08.004.
Liu, Y.-G., Miah, M.R.U., Schmitt, R.A., 1988. Cerium: A chemical tracer for paleo-oceanic redox conditions. Geochim. Cosmochim. Acta 52, 1361–1371. https://doi.org/10.1016/0016-7037(88)90207-4.
Loi, A., Cocco, F., Oggiano, G., Funedda, A., Vidal, M., Ferretti, A., Leone, F., Barca, S., Naitza, S., Ghienne, J.-F., Pillola, G.L., 2023. The Ordovician of Sardinia (Italy): from the 'Sardic Phase' to the end-Ordovician glaciation, palaeogeography and geodynamic context. Geol. Soc. Spec. Publ. 532, 409–431. https://doi.org/10.1144/SP532-2022-121.
Lumiste, K., Paiste, T., Paiste, P., Männik, P., Somelar, P., Kirsimäe, K., 2023. REE + Y uptake in bioapatite revisited: Facies-controlled variability in coeval conodonts. Chem. Geol. 640, 121761 https://doi.org/10.1016/j.chemgeo.2023.121761.
Malferrari, D., Ferretti, A., Mascia, M.T., Savioli, M., Medici, L., 2019. How much can we trust major element quantification in bioapatite investigation? ACS Omega 4, 17814–17822. https://doi.org/10.1021/acsomega.9b02426.
Manara, C., Vai, G.B., 1970. La sezione e i conodonti del costone sud del M. Rauchkofel. Giorn. Geol. 36, 441–514.
McLennan, S.M., 2001. Relationships between the trace element composition of sedimentary rocks and upper continental crust. Geochem. Geophys. Geosyst. 2 https://doi.org/10.1029/2000GC000109, 2000GC000109.
Medici, L., Savioli, M., Ferretti, A., Malferrari, D., 2021. Zooming in REE and other trace elements on conodonts: Does taxonomy guide diagenesis? J. Earth Sci. 32 (3), 501–511. https://doi.org/10.1007/s12583-020-1094-3.
Nardelli, M.P., Malferrari, D., Ferretti, A., Bartolini, A., Sabbatini, A., Negri, A., 2016. Zinc incorporation in the miliolid foraminifer *Pseudotriloculina rotunda* under laboratory conditions. Mar. Micropaleontol. 126, 42–49. https://doi.org/10.1016/j.marmicro.2016.06.001.
Negri, A., Ferretti, A., Wagner, T., Meyers, P.A., 2009a. Organic-carbon-rich sediments through the Phanerozoic: Processes, progress, and perspectives. Palaeogeogr. Palaeoclimatol. Palaeoecol. 273, 213–217. https://doi.org/10.1016/j.palaeo.2008.11.016.
Negri, A., Ferretti, A., Wagner, T., Meyers, P.A., 2009b. Phanerozoic organic-carbon-rich marine sediments: Overview and future research challenges. Palaeogeogr. Palaeoclimatol. Palaeoecol. 273, 218–227. https://doi.org/10.1016/j.palaeo.2008.10.002.
Nothdurft, L.D., Webb, G.E., Kamber, B.S., 2004. Rare earth element geochemistry of Late Devonian reefal carbonates, Canning Basin, Western Australia: confirmation of a seawater REE proxy in ancient limestones. Geochim. Cosmochim. Acta 68, 263–283. https://doi.org/10.1016/S0016-7037(03)00422-8.
Nozaki, Y., Zhang, J., Amakawa, H., 1997. The fractionation between Y and Ho in the marine environment. Earth Planet. Sci. Lett. 148, 329–340. https://doi.org/10.1016/S0012-821X(97)00034-4.
Pattan, J.N., Pearce, N.J.G., Mislankar, P.G., 2005. Constraints in using Cerium-anomaly of bulk sediments as an indicator of paleo bottom water redox environment: A case study from the Central Indian Ocean Basin. Chem. Geol. 221, 260–278. https://doi.org/10.1016/j.chemgeo.2005.06.009.
Peppe, D.J., Reiners, P.W., 2007. Conodont (U–Th)/He thermochronology: Initial results, potential, and problems. Earth Planet. Sci. Lett. 258, 569–580. https://doi.org/10.1016/j.epsl.2007.04.022.
Picard, S., Lécuyer, C., Barrat, J.-A., Garcia, J.-P., Dromart, G., Sheppard, S.M.F., 2002. Rare earth element contents of Jurassic fish and reptile teeth and their potential relation to seawater composition (Anglo-Paris Basin, France and England). Chem. Geol. 186, 1–16. https://doi.org/10.1016/S0009-2541(01)00424-7.
Prakash, S., Mahesh, C., Gairola, R.M., 2012. Sea Level Anomalies in the Tropical Indian Ocean during Two Contrasting Southwest Monsoon Years. Int. J. Ocean Clim. Syst. 3, 127–133. https://doi.org/10.1260/1759-3131.3.2.127.
Reynard, B., Lécuyer, C., Grandjean, P., 1999. Crystal-chemical controls on rare-earth element concentrations in fossil biogenic apatites and implications for paleoenvironmental reconstructions. Chem. Geol. 155, 233–241. https://doi.org/10.1016/S0009-2541(98)00169-7.
Schönlaub, H.P., 1971. Zur Problematik der Conodonten-Chronologie an der Wende Ordoviz/Silur mit besonderer Berücksichtigung der Verhältnisse im Llandovery. Geol. Palaeontol. 5, 35–57.
Schönlaub, H.P., Ferretti, A., 2015. Uqua Formation. Abh. Geol. Bundesanst. 69, 38–41.
Schönlaub, H.P., Corradini, C., Corriga, M.G., Ferretti, A., 2017. Chrono-, litho- and conodont bio-stratigraphy of the Rauchkofel Boden Section (Upper Ordovician-Lower Devonian), Carnic Alps, Austria. Newsl. Stratigr. 50, 445–469. https://doi.org/10.1127/nos/2017/0391.
Serpagli, E., 1967. I conodonti dell'Ordoviciano Superiore (Ashgilliano) delle Alpi Carniche. Boll. Soc. Paleontol. Ital. 13, 17–98.
Serpagli, E., Greco, A., 1965a. Documentazione paleontologica di Ashgilliano (Ordoviciano sup.) nel versante S del M. Zérmula (Alpi Carniche italiane). Atti Mem. Accad. Naz. Sc. Lett. Art. Modena VI, 1–12.
Serpagli, E., Greco, A., 1965b. Osservazioni preliminari su alcuni Conodonti ordoviciani e siluriani delle Alpi Carniche italiane. Boll. Soc. Paleontol. Ital. 3, 192–211.
Shen, J., Algeo, T.J., Zhou, L., Feng, Q., Yu, J., Ellwood, B., 2012. Volcanic perturbations of the marine environment in South China preceding the latest Permian mass extinction and their biotic effects. Geobiology 10, 82–103. https://doi.org/10.1111/j.1472-4669.2011.00306.x.
Sholkovitz, E., Shen, G.T., 1995. The incorporation of rare earth elements in modern coral. Geochim. Cosmochim. Acta 59, 2749–2756. https://doi.org/10.1016/0016-7037(95)00170-5.
Skinner, H.C.W., 2005. Biominerals. Mineral. Mag. 69, 621–641. https://doi.org/10.1180/0026461056950275.
Soyol-Erdene, T.-O., Huh, Y., 2013. Rare earth element cycling in the pore waters of the Bering Sea Slope (IODP Exp. 323). Chem. Geol. 358, 75–89. https://doi.org/10.1016/j.chemgeo.2013.08.047.
Stache, G., 1884. Über die Silurbildungen der Ostalpen nebst Bemerkungen über die Devon-, Carbon- und Permschichten dieses Gebietes. Z. Dtsch. Geol. Ges. 36, 277–378.
Sweet, W.C., Bergström, S.M., 1984. Conodont provinces and biofacies of the Late Ordovician. Sp. Pap. Geol. Soc. Am. 196, 69–87.
Teichmüller, R., 1931. Alte und junge Krustenbewegungen im südlichen Sardinien (Zur Geologie des Thyrrhenisgebietes). Abh. Ges. d. Wiss. Göttingen, Math. Phys. Kl. 3, 857–950.
Toyoda, K., Tokonami, M., 1990. Diffusion of rare-earth elements in fish teeth from deep-sea sediments. Nature 345, 607–609. https://doi.org/10.1038/345607a0.
Trotter, J.A., Eggins, S.M., 2006. Chemical systematics of conodont apatite determined by laser ablation ICPMS. Chem. Geol. 233, 196–216. https://doi.org/10.1016/j.chemgeo.2006.03.004.
Trotter, J.A., Gerald, J.D.F., Kokkonen, H., Barnes, C.R., 2007. New insights into the ultrastructure, permeability, and integrity of conodont apatite determined by transmission electron microscopy. Lethaia 40, 97–110. https://doi.org/10.1111/j.1502-3931.2007.00024.x.
Trotter, J.A., Barnes, C.R., McCracken, A.D., 2016. Rare earth elements in conodont apatite: Seawater or pore-water signatures? Palaeogeogr. Palaeoclimatol. Palaeoecol. 462, 92–100. https://doi.org/10.1016/j.palaeo.2016.09.007.
Trueman, C.N., Tuross, N., 2002. Trace Elements in Recent and Fossil Bone Apatite. Rev. Mineral. Geochem. 48, 489–521. https://doi.org/10.2138/rmg.2002.48.13.
Vai, G.B., Spalletta, C., 1980. The Uggwa section. In: Schönlaub, H.P. (Ed.), Second European Conodont Symposium (ECOS II) Guidebook Abstracts. Abh. Geol. B.-A, vol. 35, pp. 48–50.
Walliser, O.H., 1964. Conodonten des Silurs. Abh. Hess. Landesamt. Bodenf. 41, 1–106.
Webb, G.E., Kamber, B.S., 2000. Rare earth elements in Holocene reefal microbialites: a new shallow seawater proxy. Geochim. Cosmochim. Acta 64, 1557–1565. https://doi.org/10.1016/S0016-7037(99)00400-7.
Webb, G.E., Nothdurft, L.D., Kamber, B.S., Kloprogge, J.T., Zhao, J.-X., 2009. Rare earth element geochemistry of scleractinian coral skeleton during meteoric diagenesis: a sequence through neomorphism of aragonite to calcite. Sedimentology 56, 1433–1463. https://doi.org/10.1111/j.1365-3091.2008.01041.x.
Wright, J., Colling, A., 1995. Seawater: Its Composition, Properties, and Behaviour, Second edition. Pergamon Press, in association with the Open University, Oxford, p. 168. https://doi.org/10.1016/C2013-0-10208-5.
Wright, J., Schrader, H., Holser, W.T., 1987. Paleoredox variations in ancient oceans recorded by rare earth elements in fossil apatite. Geochim. Cosmochim. Acta 51, 631–644. https://doi.org/10.1016/0016-7037(87)90075-5.
Yan, X.-P., Kerrich, R., Hendry, M.J., 1999. Sequential leachates of multiple grain size fractions from a clay-rich till, Saskatchewan, Canada: implications for controls on the rare earth element geochemistry of porewaters in an aquitard. Chem. Geol. 158, 53–79. https://doi.org/10.1016/S0009-2541(99)00011-X.

Zapanta LeGeros, R., 1981. Apatites in biological systems. Prog. Cryst. Growth Charact. 4, 1–45. https://doi.org/10.1016/0146-3535(81)90046-0.
Zhang, J., Nozaki, Y., 1996. Rare earth elements and yttrium in seawater: ICP-MS determinations in the East Caroline, Coral Sea, and South Fiji basins of the western South Pacific Ocean. Geochim. Cosmochim. Acta 60, 4631–4644. https://doi.org/10.1016/S0016-7037(96)00276-1.
Zhang, J., Amakawa, H., Nozaki, Y., 1994. The comparative behaviors of yttrium and lanthanides in the seawater of the North Pacific. Geophys. Res. Lett. 21, 2677–2680. https://doi.org/10.1029/94GL02404.
Zhang, K., Shields, G.A., 2022. Sedimentary Ce anomalies: Secular change and implications for paleoenvironmental evolution. Earth Sci. Rev. 229, 104015 https://doi.org/10.1016/j.earscirev.2022.104015.
Zhang, L., Algeo, T.J., Cao, L., Zhao, L., Chen, Z.-Q., Li, Z., 2016. Diagenetic uptake of rare earth elements by conodont apatite. Palaeogeogr. Palaeoclimatol. Palaeoecol. 458, 176–197. https://doi.org/10.1016/j.palaeo.2015.10.049.
Zhao, L., Chen, Z.-Q., Algeo, T.J., Chen, J., Chen, Y., Tong, J., Gao, S., Zhou, L., Hu, Z., Liu, Y., 2013. Rare-earth element patterns in conodont albid crowns: Evidence for massive inputs of volcanic ash during the latest Permian biocrisis? Glob. Planet. Chang. 105, 135–151. https://doi.org/10.1016/j.gloplacha.2012.09.001.
Žigaitė, Ž., Fadel, A., Blom, H., Perez-Huerta, A., Jeffries, T., Märss, T., Ahlberg, P.E., 2015. Rare earth elements (REEs) in vertebrate microremains from the upper Pridoli Ohesaare beds of Saaremaa Island, Estonia: geochemical clues to palaeoenvironment. Eston. J. Earth Sci. 64 (1), 115–120. https://doi.org/10.3176/earth.2015.21.
Žigaitė, Ž., Fadel, A., Perez-Huerta, A., Jeffries, T., Goujet, D., Ahlberg, P.E., 2016. Paleoenvironments revealed by rare-earth element systematics in vertebrate bioapatite from the Lower Devonian of Svalbard. Can. J. Earth Sci. 53 (8), 788–794. https://doi.org/10.1139/cjes-2015-0206.
Žigaitė, Ž., Qvarnström, M., Bancroft, A., Pérez-Huerta, A., Blom, H., Ahlberg, P.E., 2020. Trace and rare earth element compositions of Silurian conodonts from the Vesiku Bone Bed: Histological and palaeoenvironmental implications. Palaeogeogr. Palaeoclimatol. Palaeoecol. 549, 109449 https://doi.org/10.1016/j.palaeo.2019.109449.

Further reading

Ferretti, A., Serpagli, E., Leone, F., Loi, A., 1998b. The late Ordovician section Cea Brabetza near San Basilio. Giorn. Geol. 60 (Spec. Issue), 96–101.